Indian Journal of Advances in Chemical Science

Article

# Doxorubicin Conjugated Reduced Graphene Oxide Embedded Carboxymethyl Chitosan and Sodium Alginate-based pH Responsive Composite Beads for Synergistic Anticancer Effect

**B. Adilakshmi[1], D. Hemalatha[1], O. Sreekanth Reddy[2], K.S.V. Krishna Rao[1]***

*[1]Department of Chemistry, Yogi Vemana University, Kadapa, Andhra Pradesh, India, [2]Department of Chemistry, Sri Krishnadevaraya University, Ananthapuramu, Andhra Pradesh, India*

**ABSTRACT**

Polymeric drug delivery systems (DDS) were developed to increase half-life and bioavailability, making them ideal for biocompatible targeted drug delivery. Hence, instead of using traditional treatment methods such as surgery, chemotherapy, and radiation, polymeric therapeutics have been used to reduce adverse effects. To address this need, the present work develops the potential natural bionanocomopsite from reduced graphene oxide, carboxymethyl chitosan, and sodium alginate DDS by the facile gelation technique for the targeted delivery of two anti-cancer drugs (5-fluorouracil and doxorubicin). These bionanocomposites are characterized by the Fourier-transform infrared spectroscopy, X-ray diffraction, differential scanning calorimetry, thermogravimetric analysis, and scanning electron microscopic, further evaluated the drug loading and entrapment efficiency. The *in vitro* drug release characteristics of drugs were performed in pH 1.2 and 7.4 at 37°C. *In vitro* cytotoxicity experiments of bionanocomposites against MCF-7 (breast cancer cell line), results indicate that the highest rate of cancer cell death occurred compared to pure doxorubicin. This research not only provides rationale for enhancing a DDS tailored to MCF-7, but also suggests that DOX-rGO may be a potential therapeutic delivery vehicle.

**Key words:** Doxorubicin, Graphene oxide, Chitosan, Sodium Alginate, pH responsive polymers, Anti-cancer.

## 1. INTRODUCTION

In many parts of the world, cancer ranks high on the list of leading killer diseases. At 8.8 million, cancer was the second leading cause of death worldwide in 2020 [1]. Roughly one in six deaths in the world is caused by cancer. About 70% of deaths in low- and middle-income countries are caused by cancer. Tumors can be treated with a variety of surgical, chemical, radiation, hormonal, targeted, and even synthetic lethal methods. The biodistribution of the chemotherapeutic compound poses a significant problem in cancer chemotherapy because it can lead to serious toxicities and unwanted effects in unintended tissues. One promising strategy for addressing these limitations is the development of a delivery system that can differentially administer antitumor doses of chemotherapeutic drugs to cancer [1].

Cancer cells rapidly acquire resistance to drugs, so the use of a single drug rarely achieves sufficient treatment effectiveness. Codelivery of multi-functional agents is a promising approach that has piqued the interest of the cancer research community as a means to address this issue and boost antitumor activity. Tumor heterogeneity is attributed to the fact that cancer can develop at any point in the cell cycle, and that different anti-tumor drugs are effective against tumors at different stages of the cell cycle. The combination of two or more chemotherapeutic agents in a delivery vehicle could have a synergistic effect on cells at different stages of development. Therefore, coadministration would overcome drug resistance in tumor cells and greatly enhance treatment efficacy in comparison to single drug agents. However, the combination therapy can be affected by the associated complications, which can worsen the patient's health. The introduction of tumor-specific activity has alleviated this worry by not only reducing adverse reactions but also enhancing treatment. Therefore, it has been one of the most appealing and effective multimodal treatment strategies [2].

Hydrogels beads are polymeric networks made of hydrophilic and/or non-hydrophilic polymers that can absorb large volumes of water or biological fluids without becoming soluble in the surrounding medium [2,3]. Hydrogels are a promising biomaterial, and natural polymers have recently emerged as a potential raw material for making them because of their biocompatibility and low environmental impact. In addition to their use in biomedical applications, hydrogels made from different polysaccharides have found use in a number of other industrial applications. Researchers have looked into hydrogels' potential to swell in response to environmental stimuli. The polysaccharide-based smart hydrogels have been developed for the targeted delivery of drugs, gene, and low-molecular weight proteins [4-8].

The pyrimidine analogue 5-fluorouracil (5-fluoro-2, 4-pyrimidinedione, 5-FU) is an antimetabolite. It is unique among chemotherapeutic agents in that it is effective against solid tumors throughout the body,

***Corresponding author:**
*K.S.V. Krishna Rao*
*E-mail: ksvkr@yogivemanauniversity.ac.in*

**ISSN NO:** 2320-0898 (p); 2320-0928 (e)
**DOI:** 10.22607/IJACS.2023.1102007

**Received**: 15th March 2023;
**Revised:** 10th April 2023;
**Accepted:** 11th April 2023.

including those in the gastrointestinal tract, ovaries, pancreas, liver, head, and neck, and breast [6]. Breast, colorectal, and gastric cancers are all treated with 5-FU, an anticancer medication. The half-life of this medication is only about 15–20 min. The use of nanotechnology in drug delivery has the potential to lengthen the half-life of drugs in the body [9,10]. The 5-fluorouracil (5-FU) injectable bolus injection is a commonly prescribed antitumor agent in colorectal cancer. When given intravenously, the cytotoxic drug 5-FU may cause stomach and bowel problems. Site-specific oral distribution of 5-FU for colon cancer patients may help with these symptoms.

The anthracycline drug doxorubicin (DOX) has been shown to be effective in treating various types of cancer, including those of the breast, ovary, prostate, brain, and cervix, as well as the lung [11]. However, its application has been hampered by issues such as cardiac toxicity, a short half-life, and a lack of water solubility. Furthermore, different DOX surface functional groups may bind to and disrupt drug molecules. Hence, functionalized DOX is an excellent system because it has higher drug adsorption capacity and greater solubility than graphene. Many scientists are working to improve DOX's transport efficiency and mitigate the drug's negative side effects. Liu *et al.* synthesized protein-modified graphene oxide to improve its therapeutic efficacy. Using graphene oxide, Yang *et al.* were able to load doxorubicin onto a non-covalent nanocarrier (DOX). In addition, experimental evidence provided by Zhang *et al.* demonstrated that the DOX molecule that was covalently bonded to DOX exhibited enhanced anti-tumor activity [12]. Carboxymethyl chitosan (CMC), a significant water-soluble chitosan derivative, it is synthesized by carboxymethylation of -OH groups of chitosan [13]. As a result, responsive ligands with -COOH and -$NH_2$ groups can still chemically improve their physicochemical properties for bonding with drugs, chelating metal ions, and dye binding. It has several notable properties, including non-toxicity, degradability, biocompatibility, antibacterial, and antifungal bioactivity. Furthermore, carboxymethylation as a hydrophilic modification can improve chitosan solubility, due to these advantages. CMC has gotten a lot of attention in the biomedical field, such as wound healing, bioimaging, tissue engineering, and drug/gene delivery. Sodium alginate (SA) is an anionic polymer, which is extracted from brown seaweed and possesses the property of being hydrophilic [14,15]. Because of its low risk to biological systems, it can be used effectively in the targeted delivery of drugs. It is made up of D-mannuronic acid and L-guluronic acid that is structured in the form of alternating blocks of MM or GG and MG, as stated in. Because of its exceptional properties, such as biocompatibility, biodegradability, non-toxicity, and a hydrophilic nature, SA is a good candidate for use as a drug delivery vehicle in a variety of biomedical applications [14].

In signal transduction and metabolism, reactive oxygen species (ROS) play a critical role [16]. When ROS levels are too high in cells or tissues (as is the case with ROS overproduction), oxidation stress can occur, which has been linked to a wide range of diseases, including cancer. On-demand drug delivery and the recent development of ROS-responsive materials and nanomedicine have piqued researchers' interest in responsive drug delivery systems (DDSs). Using ROS-responsive DDS, therapeutic agents can be released only in areas where ROS levels are excessively high, potentially enhancing healing efficiency while minimizing side effects [16,17]. By consideration of importance of targeted DDSs, the present work aims to design a potential tumor-targeted DDS, that is, doxorubicin conjugated reduced graphene oxide embedded CMC and SA-based pH responsive composite beads. These systems are expected to have specificity as well as high drug loading efficiency for tumor-targeting drug delivery.

## 2. MATERIALS AND METHODS

### *2.1. Materials*

Chitosan (low molecular weight, Mw = 800,000 Da), 5-fluorouracil, 1-ethyl-3-[3-dimethylaminopropyl]carbodiimide hydrochloride (EDC), N-hydroxysuccinimide (NHS), and ethylenediamine were obtained from sigma Aldrich (St. Louis, MO, USA). Sodium hydroxide, graphite, sodium nitrate, sulfuric acid, potassium permanganate, 30% (v/v) hydrogen peroxide, hydrazine sulfate, isopropanol, methanol, ethanol, glacial acetic acid, and monochloroacetic acid were purchased from SD fine chemicals Ltd. (Mumbai, India). Doxorubicin hydrochloride (DOX) was obtained from Aspire Pharma (Telangana, India). Double distilled water was used throughout the experiments.

### *2.2. Synthesis of CMC*

CMC was synthesized as per the published procedure [18], in brief, 6 g of chitosan was added to 100 mL of isopropanol stirred 30 min at 300 rpm, then 30 mL of a sodium hydroxide (10 M) solution was added drop by drop, followed by 15 mL of a 10% (v/v) monochloroacetic acid. Reaction allowed for 6 h at 50°C, then 100 mL of methanol was added. The slurry had been filtered. The obtained solid was washed thoroughly with 80 % (v/v) ethanol and dried at 40°C in hot air oven.

### *2.3. Synthesis of Reduced Graphene Oxide-DOX Conjugates*

Reduced graphene oxide was dissolved in 150 g/mL DI distilled water and sonicated for 30–60 min to reduce the size for effective cell internalisation. After 60 min, they were centrifuged and dried. 4 mg of NHS and 6 mg of N-(3-dimethylaminopropyl)-N'-ethylcarbodiimide hydrochloride were added after dispersing 150 mg of reduced graphene oxide in 20 mL of phosphate buffer (0.1 M, pH 6.0). After 30 min of bubbling, the mixture was allowed to react with 15 mg of doxorubicin at room temperature for 48 h in phosphate-buffer (pH 6.0). After centrifugation, the DOX-rGO was washed three times with distilled water before being dried.

### *2.4. Preparation of Polymeric Drug Hydrogel Beads*

The heteroionic gelation method was used to create polymeric blend hydrogel beads (SA and CMC). Polymeric blend hydrogel beads were created by combining DOX, rGO-DOX and 5FU in various ratios [Table 1]. SA (0.02 g) was dissolved in 10 mL of deionized water at room temperature and stirred for 2 h to make hydrogel beads. In contrast, CMC solution was made by dissolving CMC (5%) in 10 mL deionized water and stirring constantly at room temperature until homogeneous. The resulting blended solution with various rGO-DOX/5FU compositions was stirred for 2 h at room temperature before being dropped into the $CaCl_2$ solution. Resulted beads are dried at 40°C in thermally controlled hot air oven. Schematic representation of preparation beads is shown in **Scheme 1**.

### *2.5.Characterization Techniques*

Using the KBr pellet method, additional details about the structure and the rGO-DOX and drug-polymer interactions were acquired using an FT-IR spectrophotometrically in the 4000–400 $cm^{-1}$ range at a resolution of 0.5 $cm^{-1}$. SEM was used to examine the morphological characteristics of created microbeads (S4800, Hitachi, Japan). Thermogravimetric analysis (TGA) was used to determine the thermal properties of synthesized samples. Powder X-ray diffraction (PXRD) of samples was performed on a powder diffractometer system (Ultima IV, Rigaku, Japan) and scans were recorded at a scan rate of 10°/min using Cu K radiation.

### *2.6. In Vitro Drug Release*

The *in vitro* release profiles of all drug-loaded carriers were analyzed by performing dissolution experiments. 10 mg of drug-loaded microbeads were kept in a dialysis bag and transferred into 50 mL of

**Table 1:** Formulation and composition of all samples used for the studies

| Code | SA (mg) | CMC (mg) | 5-Fu (mg) | DOX (mg) | rGO-DOX (mg) | $CaCl_2$ (%) |
|---|---|---|---|---|---|---|
| CMCSA5FU | 200 | 10 | 20 | --- | ---- | 0 |
| CMCSADC | 200 | 10 | --- | --- | 20 | 0 |
| CMCSADOX | 200 | 10 | --- | 20 | --- | 2.5 |
| CMCSADC+5-FU | 200 | 20 | 20 | --- | 20 | 0 |
| CMCSA+5-FU+DOX | 200 | 30 | 20 | 20 | --- | 0 |
| Placebo | 200 | 000 | 00 | 5 | 0 | 0 |

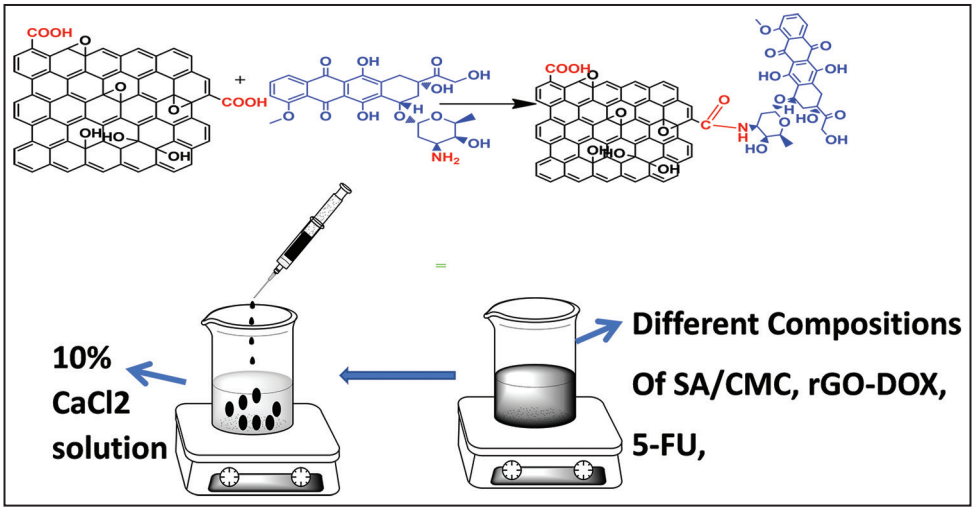


**Scheme 1:** Schematic representation doxorubicin conjugated reduced graphene oxide conjugated doxorubicin embedded carboxymethyl chitosan and sodium alginate-based pH responsive composite beads.

PBS (pH 1.2 and 6.8) media and agitated at 50 rpm at 37°C. 2 mL of dissolution media was taken out at regular intervals and measured with a UV-visible spectrophotometer set to 280 and 481 nm for 5-FU and DOX, respectively. The same amount was then filled with new media.

### *2.7. Cytotoxic and Reactive Oxygen Species (ROS) Studies*

The cell viability of conjugate of DOX-rGO, drug loaded (5-FU and DOX) CMC+SA beads, and conjugate DOX-rGO loaded microbeads were examine using MTT assay. In brief MCF-7 cells were added and incubated in 96 well plate. Various amounts of drug conjugated and drug loaded SA/CMC hydrogel beads were introduced to the cells, after that the cells were incubated for overnight and followed by suspension was withdrawn and MTT solution was added. After another hours, the media was removed and formazan crystals were lysed with DMSO. Finally, the absorption spectrum measured at 570 nm with spectrophotometric microplate reader. MCF7-human breast tumour cells were collected from the National Centre for Cell Science (NCCS, Pune, India), and MTT study was carried out at Stellixir Biotech Pvt Ltd, Bangalore, India. The ROS-generating capacity of a sample was analyzed using 2,7-dichlorodihydrofluorescein diacetate ($H_2$DCFDA) as described in an earlier study [19].

## 3. RESULTS AND DISCUSSIONS

### *3.1. Fourier-Transform Infrared Spectroscopy (FTIR) Studies*

FTIR spectra [Figure 1] of rGO show peaks at 3321 $cm^{-1}$ (O–H stretching frequency), 1723 $cm^{-1}$ (C=O stretching frequency), 1574 $cm^{-1}$ (C=C stretching frequency), and 1123 $cm^{-1}$ (C–O–C stretching frequency). The spectrum of DOX shows peaks at 3325 $cm^{-1}$ (due to stretching vibrations of O–H and N–H), 1731 $cm^{-1}$ (due to stretching vibrations of C=O), 1388 $cm^{-1}$ (due to bending vibrations of O–H), 1589 $cm^{-1}$ (due to

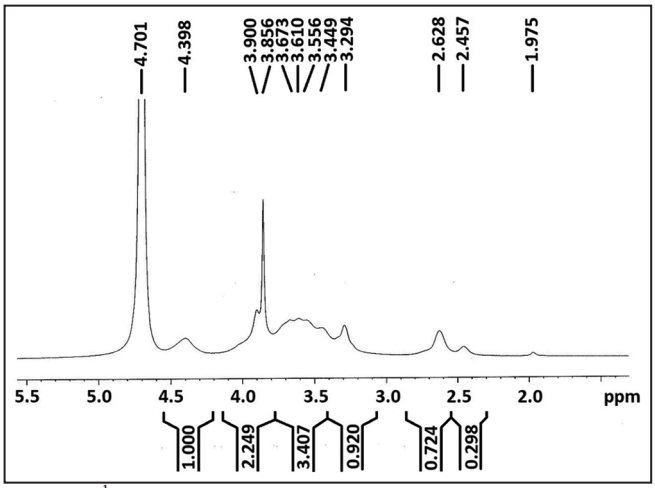


**Figure 1:** $^1$H NMR spectrum of carboxymethyl chitosan.

bending vibrations of N–H), 1072 $cm^{-1}$ (due to stretching vibrations of C–O), 1288 $cm^{-1}$ (due to stretching vibrations of C–N), 995 $cm^{-1}$ (due to bending vibrations of C=C), and 802 $cm^{-1}$ (due to bending vibrations of C–H). The C=O group of rGO and $NH_2$ group of doxorubicin diminished on conjugation of doxorubicin, and this was accompanied by appearance of amide I and II bands [Figure 2], implying successful conjugation of doxorubicin by the reaction of $NH_2$ groups of DOX with the COOH groups of rGO. The additional new peaks below 1,500 $cm^{-1}$ observed in spectrum could be readily assigned to DOX by referring to the FTIR spectrum for free DOX, further confirming the successful conjugation of DOX with the rGO. After the incorporation of rGO-DOX in polymer matrix, new peak at 1499 $cm^{-1}$ (NH-C=O vibration), suggesting that

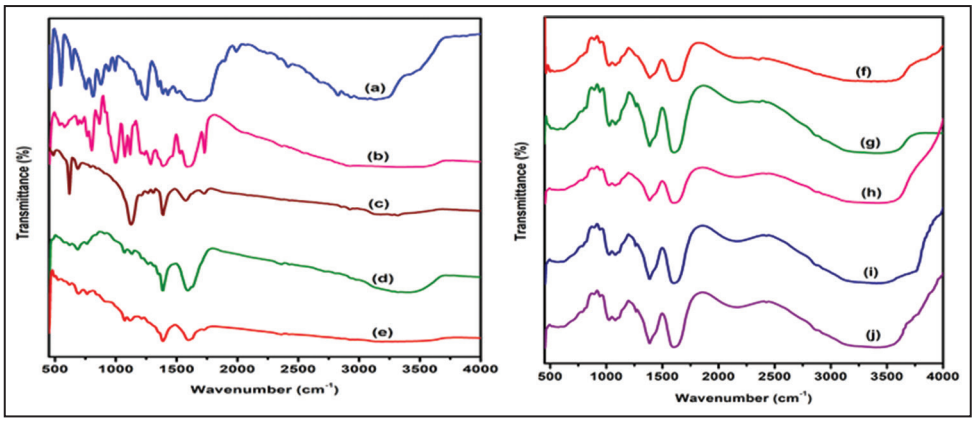


**Figure 2:** Fourier-transform infrared spectroscopy spectrum of (a) 5-FU (b) DOX (c) rGO (d) rGO-DOX (e) SAMCS (f) SAMCS -rGO-DOX (g) SAMCS -5FU (h) SAMCS-DOX (i) SAMCS -5FU-DOX (j) SAMCS -rGO-DOX-5-FU.

the drug conjugate was effectively loaded into the polymeric beads, and also the rGO peak at 1730 $cm^{-1}$ was disappeared in the beads, indicating that the C=O group of rGO has interacted with polymer matrix and 5-FU molecules, these results confirmed the successfully encapsulation of 5-FU in polymer beads [19]. The spectrum of CMC shows peaks at 3207 $cm^{-1}$ and 3433 $cm^{-1}$ for –OH and –NH stretching vibrations, respectively. Peaks at 2923 $cm^{-1}$ (due to C–H stretching vibrations), 1601 $cm^{-1}$ (due to symmetric axial deformation of –COOH) and 1392 $cm^{-1}$ (due to asymmetric axial deformation of –COOH) confirm the existence of carboxymethyl groups on chitosan. Peaks at 1064 $cm^{-1}$ and 1111 $cm^{-1}$ are assigned to C–O-C stretching vibrations, indicating the existence of carbonyl groups. FTIR spectra of 5-FU show the peaks at 3009–3139 $cm^{-1}$ (N–H and C–H stretching frequency) 1665 $cm^{-1}$ (C=O stretching frequency), and 1245 $cm^{-1}$ (C–F stretching frequency) [20]. FTIR spectrum of SA shows a peak at 1600 $cm^{-1}$ (symmetric stretching vibrations of –COOH) and 1413 $cm^{-1}$ (antisymmetric stretching vibration of -COOH), 3510 $cm^{-1}$ (-OH stretching vibration), 2905 $cm^{-1}$ (-$CH_2$ stretching vibration), and 1010–1100 $cm^{-1}$ (-C-O-C stretching frequency). Similarly, in the case of SAMCS-5FU, SAMCS -DOX, SAMCS -5FU-DOX, and SAMCS -5FU-DOX conjugate, microbeads, C–F and 1350 $cm^{-1}$ (C-O- C stretching vibration), 2970 $cm^{-1}$ (aromatic C-C stretching frequency), and 1596 $cm^{-1}$ (C=O stretching vibration) of CMC. These stretching frequencies were indicating that both 5-FU and DOX were present in the polymeric beads.

### *3.2. XRD Studies*

The XRD patterns of the pristine rGO, DOX, and 5-FU and polymeric beads are shown in the Figure 3. The pristine rGO, DOX, and 5-FU XRD crystalline peaks (20 and 30° for rGO and DOX; 28.68° for 5-FU). These crystalline peaks are not appeared in the polymeric beads and drug loaded beads, these results indicate that rGO-DOX conjugate and 5-FU are molecularly dispersed and also beads are in amorphous state.

### *3.3. SEM Studies*

SEM images of drug (DOX and 5-FU) loaded polymeric beads are shown in Figure 4. The SEM images show that polymeric beads are slightly rough surface, randomly arrayed, and extremely porous. There are drug crystals on the surfaces of the beads, indicating that the drug is distributed molecularly throughout the beads. The average diameter of polymeric beads was ~282.71 mm.

### *3.4. Thermal Analysis*

The TGA [Figure 5] curve of rGO reveals that appearance of two distinct weight loss phases, first occurring between 35°C and 151°C and resulting in a weight loss of 27%, and the second occurring between 215°C and

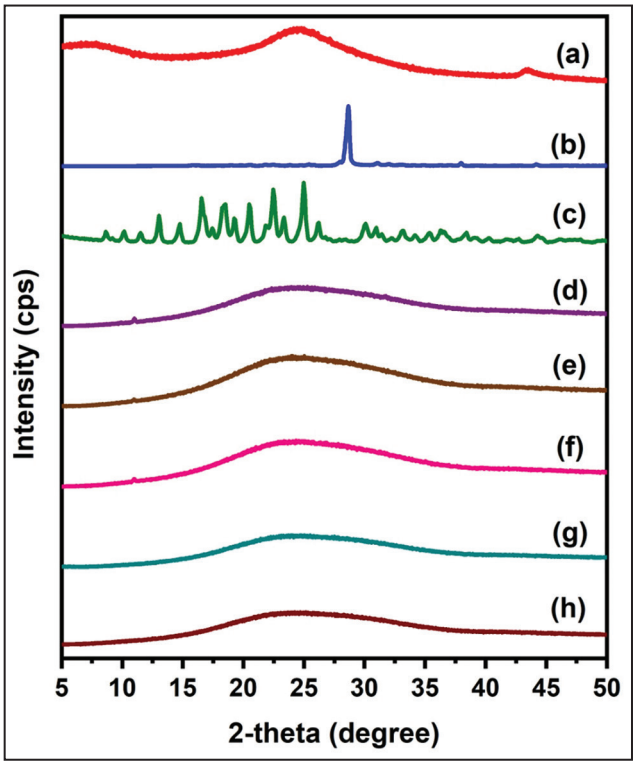


**Figure 3:** X-ray diffraction patterns of (a) rGO (b) 5-FU (c) DOX (d) SAMCS hydrogel beads (e) SAMCS-rGO-DOX (f) SAMCS -5FU (g) SAMCS-DOX (h) SAMCS-rGO-DOX-5FU.

600°C and resulting in a weight loss of 36%. The first loss is due to evaporation of trace amount of moisture, while the second loss is due to the decomposition of oxygen-containing functional groups in rGO [4]. The TGA analysis of placebo beads observed four weight loss peaks, the first path was observed at 49–172.47°C with weight loss of 13% due to its loss of moisture. The second path is observed at 183–248°C with weight loss of 17%, the third path is observed at 254.12–363.19°C with weight loss 12%, the last path observed at 397–600°C with weight loss of 4.16% due to degradation of polymer matrix. The TGA characterization of drug conjugate shows one weight loss peak, which is observed at 93–596.746°C with weight loss 53.142% due to dehydration of water molecules and degradation of polymeric chains. The TGA analysis of SAMCS + rGO-DOX has observed three different weight loss peaks were observed, the path is observed at 129–254°C with weight loss of 22.93%, which is due to dehydration of absorbed water. The second path

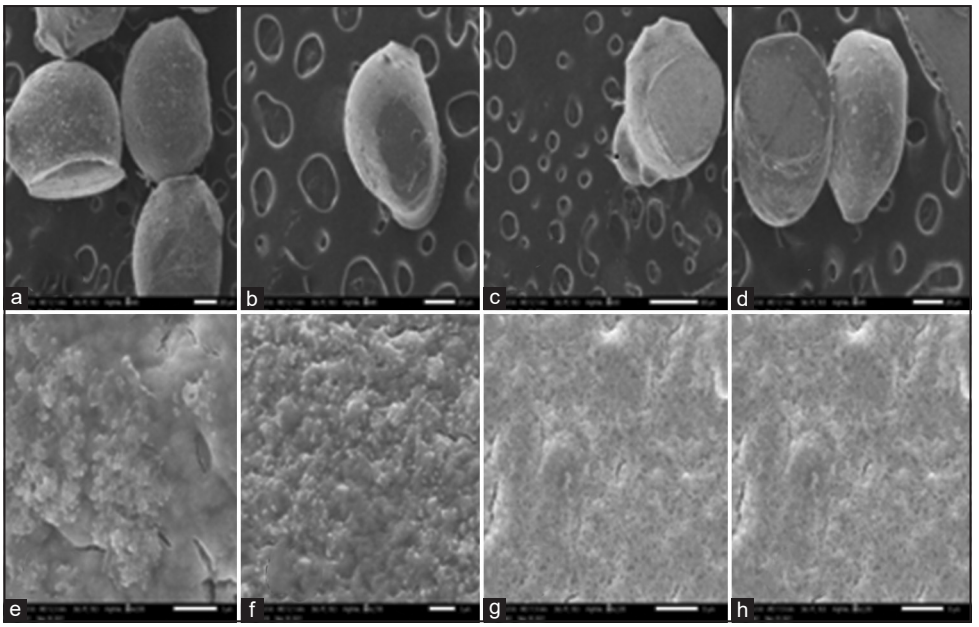


**Figure 4:** Scanning electron microscope images of (a) SAMCS-rGO-DOX (b) SAMCS-5-FU (c) SAMCS-DOX (d) SAMCS-rGO-DOX-5-FU (e-f are the surfaces to a-d).

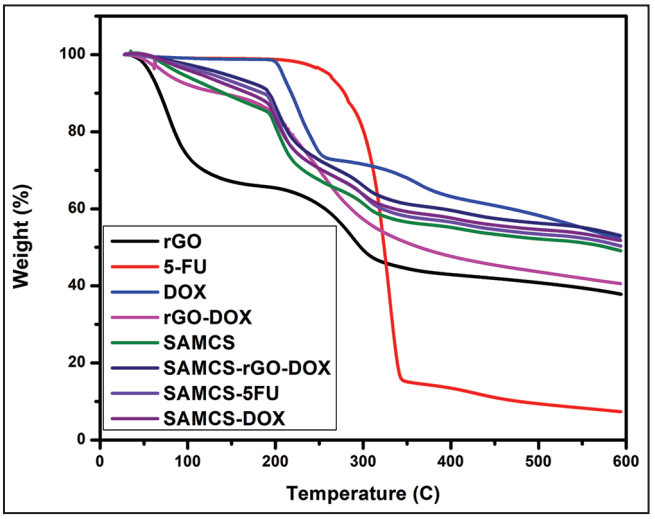


**Figure 5:** Thermogravimetric analysis curves of (a) DOX (b) 5-FU(c) rGO (d) SAMCS (e) rGO-DOX (f) SAMCS-rGO-DOX (g) SAMCS-DOX (h) SAMCS-5-FU.

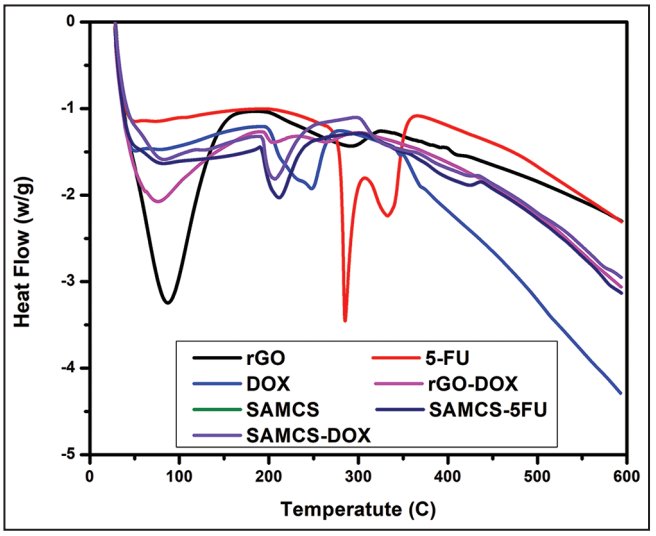


**Figure 6:** Differential scanning calorimetry curves of (a) DOX (b) 5-FU(c) rGO (d) SAMCS (e) rGO-DOX (f) SAMCS-rGO-DOX (g) SAMCS-DOX (h) SAMCS-5-FU.

is observed at 258.134–368°C with weight loss of 10.584%, the third weight loss peak was observed at 388–584.23°C with weight loss 7.33% which is due to degradation of oxygen containing functional groups.

The TGA analysis of SAMCS+5-FU has two significant weight loss paths, first one is 155.951–241.61°C with weight loss is 21.2% due to loss of water molecules, the second path is observed at 255.4–335.6°C with weight loss 10.5%, which is due to degradation of polymer matrix. Differential scanning calorimetry (DSC) [Figure 6] of pure DOX and 5-FU showed peaks at 194 and 285°C, respectively, which corresponds to the melting endotherm of drugs. This peak was not found in the drug-loaded/conjugated hydrogel beads, indicating that the 5-FU and DOX were homogeneously distributed throughout the polymer matrix.

### *3.5. In Vitro Release Studies and Release Kinetics*

To determine the releasing behavior of the drug from the polymer matrix, drug-loaded samples were treated with both simulated gastric fluid and simulated intestinal fluid. The Figure 7 clearly shows that the maximum drug release for SAMCS hydrogel beads was at pH 7.4 when compared to pH 2.0. The reason can be explained by the material's swelling capacity; at 7.4 (37°C), the carboxylic groups of SA and CMC become ionized, causing the matrix to become loose, and entrapped drug molecules to leak out easily from the polymer matrix. However, it does not swell much at acidic pHs [21,22]. As a result, the drug molecules are unable to diffuse from the polymer matrix. As the pH increased, the polymer network began to swell, allowing $H_2O$ molecules to enter the matrix and drug molecules to slowly diffuse out of the polymer matrix. At pH 7.4 (37°C), it was observed that approximately 90% of the drug is released after 24 h for SAMCS-5-FU. The drug release rate is increased and controlled at pH 2.0 rather than pH 7.4 after incorporation of rGO. This was explained by hydrogen bonding interactions between the rGO functional groups (-COOH and -OH) and the drug's N-H and O-H groups. $H^+$ ions in the medium

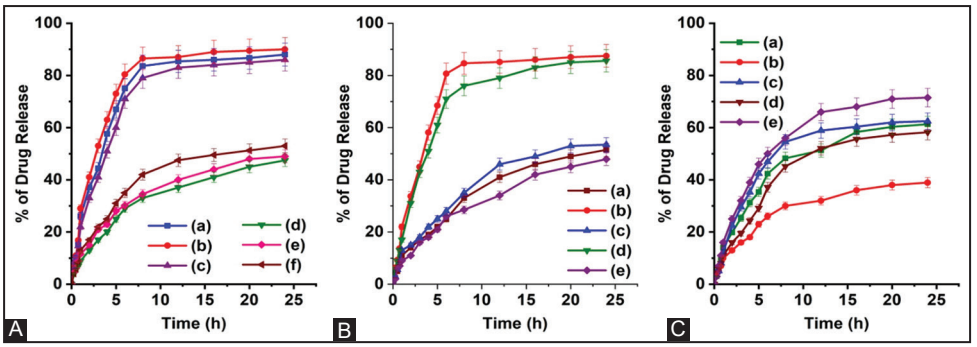


**Figure 7:** (a) 5-FU release profiles from (a) SAMCS-5-FU-DOX (b) SAMCS-5-FU, and (c) SAMCS-rGO-DOX-5-FU at pH 7.4 and (d) SAMCS-5-FU, (e) SAMCS-rGO-DOX-5-FU and (f) SAMCS-5-FU-DOX at pH2.0; (b) DOX release profiles from (a) SAMCS-rGO-DOX, (b) SAMCS-DOX, (c) SAMCS-rGO-DOX-5-FU, (d) SAMCS-5-FU-DOX and (e) rGO-DOX at pH 7.4. (c) DOX release profiles from (a) SAMCS-rGO-DOX, (b) SAMCS-DOX, (c) SAMCS-rGO-DOX-5-FU, (d) SAMCS-5-FU-DOX and (e) rGO-DOX at pH 2.0.

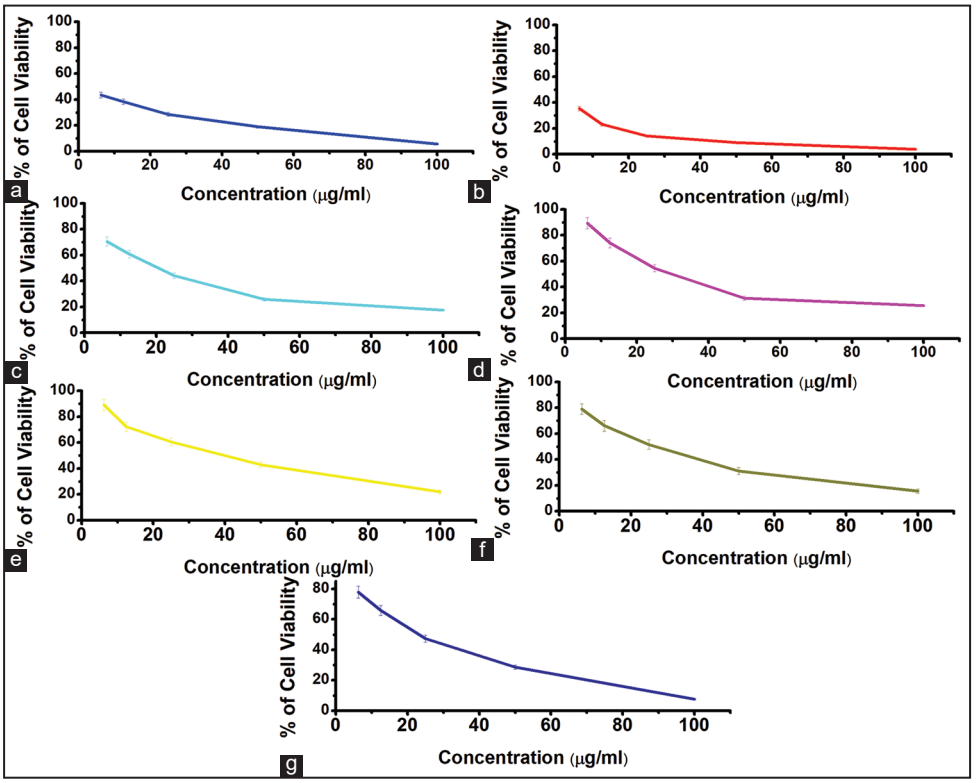


**Figure 8:** Cell viability of MCF-7 cell line against (a) 5-FU (b) DOX (c) SAMCS-rGO-DOX (d) SAMCS-5-FU (e) SAMCS-DOX (f) SAMCS-5-FU-DOX (g) SAMCS-rGO-DOX-5-FU.

disrupted hydrogen bonding interactions between rGO and the drug under acidic conditions, resulting in increased drug release. At pH 2.0, it was observed that approximately 87.5% of the drug is released after 24 h for SAMCS-rGO-DOX. The correlation coefficient ($r^2$) of the linear relationship between release rate and time was calculated for these models (zero-order, first order, Higuchi, and Korsmeyer-Peppas) to evaluate the release kinetic strategy, and the results are shown in the Table 2. As a correlation coefficient approaching 0.90 was observed, it can be concluded that the Korsmeyer-Peppas model.

It was the best appropriate model for understanding the kinetics of drug release from produced carriers. In the Korsmeyer-Peppas model, the *n* value describes the releasing mechanism. In the present study, the *n* values of developed carriers ranged between 0.560 and 0.785, indicating non-Fickian release or anomalous transport, and the diffusion through polymer matrix relaxation was the most important factor in determining drug release.

### *3.6. In Vitro Cytotoxicity, ROS and Biocompatibility*

Cytotoxicity tests were carried out on MCF-7 cells at various concentrations (6.25, 12.5, 25, 50, and 100 g/mL) and the results are shown in Figure 7. Due to the presence of a conjugate system and 5-FU, the MTT results revealed that the compositions SAMCS-rGO-DOX-5-FU had a higher inhibitory action (percent cell viability 9.6%, respectively) on MCF7 than the other compositions. In contrast to SAMCS-rGO-DOX (32% cell viability), SAMCS-5-FU-DOX (30%) demonstrated excellent inhibitory effectiveness due to the presence of dual drugs [23], which increases the EE of 5-FU and the antitumor property of rGO. This study discovered that the

**Table 2:** Release kinetics parameters of all formulations at pH 6.8 and pH 1.2.

| Code | Drug | pH | Korsmeyer-Peppas | | Zero Order | | First Order | | Higuchi | |
|---|---|---|---|---|---|---|---|---|---|---|
| | | | $n$ | $r^2$ | $K_0$ | $r^2$ | $K_1$ | $r^2$ | $K_H$ | $r^2$ |
| SAMCS-rGO-DOX | DOX | 7.4 | 0.560 | 0.980 | 2.704 | 0.752 | 0.039 | 0.894 | 10.84 | 0.982 |
| | | 2.0 | 0.707 | 0.991 | 3.465 | 0.514 | 0.039 | 0.894 | 10.84 | 0.982 |
| SAMCS-rGO-DOX-5-FU | DOX | 7.4 | 0.802 | 0.997 | 5.362 | 0.145 | 0.215 | 0.959 | 22.75 | 0.814 |
| | | 2.0 | 0.606 | 0.986 | 2.173 | 0.464 | 0.215 | 0.959 | 22.753 | 0.814 |
| | 5-FU | 7.4 | 0.683 | 0.988 | 5.548 | 0.468 | 0.253 | 0.969 | 23.745 | 0.783 |
| | | 2.0 | 0.596 | 0.993 | 2.692 | 0.526 | 0.040 | 0.748 | 11.052 | 0.977 |
| SAMCS-5-FU-DOX | DOX | 7.4 | 0.562 | 0.977 | 2.903 | 0.700 | 0.044 | 0.876 | 11.71 | 0.979 |
| | | 2.0 | 0.764 | 0.993 | 3.681 | 0.389 | 0.044 | 0.876 | 11.713 | 0.979 |
| | 5-FU | 7.4 | 0.708 | 0.995 | 5.154 | 0.234 | 0.179 | 0.953 | 21.684 | 0.871 |
| | | 2.0 | 0.593 | 0.990 | 2.992 | 0.495 | 0.048 | 0.761 | 12.330 | 0.951 |
| SAMCS-5-FU | 5-FU | 7.4 | 0.785 | 0.998 | 5.089 | 0.298 | 0.172 | 0.953 | 21.349 | 0.877 |
| | | 2.0 | 0.717 | 0.984 | 3.262 | 0.643 | 0.172 | 0.953 | 21.349 | 0.877 |
| SAMCS-DOX | DOX | 7.4 | 0.641 | 0.981 | 2.466 | 0.761 | 0.034 | 0.885 | 9.878 | 0.987 |
| | | 2.0 | 0.710 | 0.992 | 4.128 | 0.450 | 0.0344 | 0.885 | 9.878 | 0.987 |

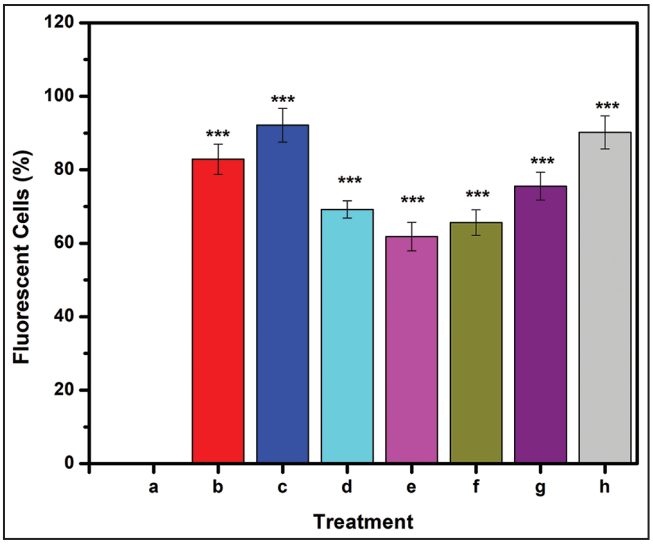


**Figure 9:** Effect of different treatments on the intracellular ROS level of MCF-7 cells as determined by the $H_2$DCFDA assay: (a) Untreated (b) 5-FU (c) DOX (d) SAMCS-rGO-DOX (e) SAMCS-5-FU (f) SAMCS-DOX(g) SAMCS-rGO-DOX-5-FU. Results denote mean ± SD ($n$ = 3 per time point). Statistical significance is calculated with respect to free drug by one-way ANOVA (***$P < 0.001$).

anticancer agents developed were effective against MCF-7 cells. The effect of microbeads on the formation of reactive oxygen species (ROS) was investigated using $H_2$DCFDA labeling; the results are depicted in Figure 8. Figure 9 shows that treatment increased the production of endogenous reactive oxygen species (ROS) in MCF-7 cells, implying that the drug-loaded carriers' antitumor effect was aided to some extent by ROS production [24,25]. ROS are important in cell death because they can orchestrate different cell death mechanisms. The aim of the study was to investigate the role of ROS in the biochemical properties of cell death induced by drug-loaded hydrogel beads [25].

## 4. CONCLUSION

We described the design and fabrication of pH sensitive hydrogel beads for controlled drug release of anti-cancer drugs (doxorubicin, DOX and 5-fluorouracil, 5-FU) using CMC and SA hydrogel beads along with reduced graphene oxide conjugated doxorubicin (rGO-DOX). FTIR, SEM, DSC, and TGA were used to examine the developed hydrogel beads. The experimental findings of formulations show that the drug-loaded hydrogel beads can effectively enter and interact with viable cancer cells. When tested against the MCF-7 cell line, rGO-DOX loaded hydrogel beads showed both high encapsulation efficiency and anticancer activity. In addition, among all composites, dual drugs (DOX and 5-FU) containing SAMCS-rGO-DOX-5-FU showed the greatest promise. In conclusion, hydrogel bead-based drug conjugation has great potential as a versatile method for creating intelligent drug delivery materials that facilitate efficient drug release and absorption. As overall, developed beads are biocompatible and have targeting potential.

## 5. ACKNOWLEDGMENTS

The author B. Adi Lakshmi is thankful to Department of Science and Technology, India for financial support under DST-INSPIRE program (IF170137).

## 6. REFERENCES

1. J. Ferlay, M. Colombet, I. Soerjomataram, D. M. Parkin, M. Piñeros, A. Znaor, F. Bray, (2021) Cancer statistics for the year 2020: An overview, ***International Journal of Cancer***, **149:** 778-789.
2. M. Cristofanilli, G. T. Budd, M. J. Ellis, A. Stopeck, J. Matera, M. C. Miller, J. M. Reuben, G. V. Doyle, W. J. Allard, L. W. M. M. Terstappen, D. F. Hayes, (2004) Circulating tumor cells, disease progression, and survival in metastatic breast cancer, ***New England Journal of Medicine***, **351:** 781-791.
3. K. S. V. K. Rao, M. C. S. Subha, B. V. K. Naidu, M. Sairam, N. M. Nadagouda, T. M. Aminabhavi, (2006) Controlled release of diclofenac sodium and ibuprofen through beads of sodium

alginate and hydroxy ethyl cellulose blends, ***Journal of Applied Polymer Science***, **102:** 5708-5718.
4. K. S. V. K. Rao, P. R. S. Reddy, K. M. Rao, C. S. Ha, (2018) Chitosan-based interpenetrating polymeric network microgels for colon specific drug delivery of 5-fluorouracil, ***Indian Journal of Advances in Chemical Science***, **6(3):** 135-141.
5. S. Eswaramma, K. S. V. K. Rao, (2017) Synthesis of dual responsive carbohydrate polymer based IPN microbeads for controlled release of anti-HIV drug, ***Carbohydrate Polymers***, **156:** 125-134.
6. G. Borchard, (2001) Chitosans for gene delivery, ***Advanced Drug Delivery Reviews***, **52:** 145-150.
7. L. M. Kranz, M. Diken, H. Haas, S. Kreiter, C. Loquai, K. C. Reuter, M. Meng, D. Fritz, F. Vascotto, H. Hefesha, C. Grunwitz, M. Vormehr, Y. Hüsemann, A. Selmi, A. N. Kuhn, J. Buck, E. Derhovanessian, R. Rae, S. Attig, J. Diekmann, R. A. Jabulowsky, S. Heesch, J. Hassel, P. Langguth, S. Grabbe, C. Huber, Ö. Türeci, U. Sahin, (2016) Systemic RNA delivery to dendritic cells exploits antiviral defence for cancer immunotherapy, ***Nature***, **534:** 396-401.
8. W. B. Parker, Y. C. Cheng, (1990) Metabolism and mechanism of action of 5-fluorouracil, ***Pharmacology and Therapeutics***, **48:** 381-395.
9. D. M. Thomas, J. R. Zalcberg, (1998) 5-fluorouracil: A pharmacological paradigm in the use of cytotoxics, ***Clinical and Experimental Pharmacology and Physiology***, **25:** 887-895.
10. K. Mross, P. Maessen, W. J. Van Der Vijgh, H. Gall, E. Boven, H. M. Pinedo, (1988) Pharmacokinetics and metabolism of epidoxorubicin and doxorubicin in humans, ***Journal of Clinical Oncology***, **6:** 517-526.
11. M. Tokarska-Schlattner, T. Wallimann, U. Schlattner, (2006) Alterations in myocardial energy metabolism induced by the anti-cancer drug doxorubicin, ***Comptes Rendus Biologies***, **329:** 657-668.
12. V. Hanušová, I. Boušová, L. Skálová, (2011) Possibilities to increase the effectiveness of doxorubicin in cancer cells killing, ***Drug Metabolism Reviews***, **43:** 540-557.
13. V. K. Mourya, N. N. Inamdara, A. Tiwari, (2010) Carboxymethyl chitosan and its applications, ***Advanced Materials Letters***, **1:** 11-33.
14. K. Nagaraja, K. M. Rao, K. S. V. K. Rao, (2021) Alginate-based hydrogels. In: T. K. Giri, B. Ghosh (Eds.), ***Plant and Algal Hydrogels for Drug Delivery and Regenerative Medicine***, Ch. 11. United Kingdom: Woodhead Publishing, p357-393.
15. S. R. Obireddy, S. Bellala, M. Chintha, A. Sake, S. M. C. Subbarao, W. F. Lai, (2023) Synthesis and properties of alginate-based nanoparticles incorporated with different inorganic nanoparticulate modifiers for enhanced encapsulation and controlled release of favipiravir, ***Arabian Journal of Chemistry***, **16:** 104751.
16. G. Saravanakumar, J. Kim, W. J. Kim, (2017) Reactive-oxygen-species-responsive drug delivery systems: Promises and challenges, ***Advanced Science*** **(*Weinh*)**, **4:** 1600124.
17. C. Xu, R. Song, P. Lu, J. Chen, Y. Zhou, G. Shen, M. Jiang, W. Zhang, (2020) A pH-responsive charge-reversal drug delivery system with tumor-specific drug release and ROS generation for cancer therapy, ***International Journal of Nanomedicine***, **15:** 65-80.
18. O. S. Reddy, W. F. Lai, (2021) Development of a composite film fabricated from carboxymethyl chitosan and magnetite nanoparticles for pH-responsive bioactive agent release, ***Biointerphases***, **16:** 021006.
19. S. R. Obireddy, W. F. Lai, (2021) Multi-component hydrogel beads incorporated with reduced graphene oxide for pH-responsive and controlled co-delivery of multiple agents, ***Pharmaceutics***, **13:** 313.
20. X. Liu, Y. Mo, X. Liu, R. Guo, Y. Zhang, W. Xue, Y. Zhang, C. Wang, S. Ramakrishna, (2016) Synthesis, characterisation and preliminary investigation of the haemocompatibility of polyethyleneimine-grafted carboxymethyl chitosan for gene delivery, ***Materials Science and Engineering C***, **62:** 173-182.
21. S. Eswaramma, K. S. V. K. Rao, (2023) Cyclotriphosphazene based stimuli-responsive semi-IPN hydrogels: Synthesis, diffusion and anti-cancer drug release characteristics, ***Indian Journal of Advances in Chemical Science***, **11(1):** 1-10.
22. S. Eswaramma, N. S. Reddy, K. S. V. K. Rao, (2017) Phosphate crosslinked pectin based dual responsive hydrogel networks and nanocomposites: Development, swelling dynamics and drug release characteristics, ***International Journal of Biological Macromolecules***, **103:** 1162-1172.
23. T. Wang, J. Hou, C. Su, L. Zhao, Y. Shi, (2017) Hyaluronic acid-coated chitosan nanoparticles induce ROS-mediated tumor cell apoptosis and enhance antitumor efficiency by targeted drug delivery via CD44, ***Journal of Nanobiotechnology***, **15:** 7.
24. E. Nyankson, S. O. Aboagye, J. K. Efavi, B. Agyei-Tuffour, L. Paemka, B. O. Asimeng, S. Balapangu, P. K. Arthur, E. K. Tiburu, (2021) Chitosan-coated halloysite nanotubes as vehicle for controlled drug delivery to MCF-7 cancer cells *in vitro*, ***Materials*** **(*Basel*)**, **14:** 2837.
25. J. X. Liao, Q. F. Huang, Y. H. Li, D. W. Zhang, G. H. Wang, (2022) Chitosan derivatives functionalized dual ROS-responsive nanocarriers to enhance synergistic oxidation-chemotherapy, ***Carbohydrate Polymers***, **282:** 119087.